IOPscience iopscience.iop.org

Home Search Collections Journals About Contact us My IOPscience

Hot-electron effect in PdAu thin-film resistors with attached cooling fins

This article has been downloaded from IOPscience. Please scroll down to see the full text article.

2009 Supercond. Sci. Technol. 22 114007

(http://iopscience.iop.org/0953-2048/22/11/114007)

View the table of contents for this issue, or go to the journal homepage for more

Download details:
IP Address: 130.89.112.87
The article was downloaded on 07/05/2010 at 08:50

Please note that terms and conditions apply.

Supercond. Sci. Technol. **22** (2009) 114007 (9pp) doi:10.1088/0953-2048/22/11/114007

Hot-electron effect in PdAu thin-film resistors with attached cooling fins

J Pleikies[1], O Usenko[2], R Stolz[3], L Fritzsch[3], G Frossati[2] and J Flokstra[1]

[1] Low Temperature Division, Faculty of Science and Technology, University of Twente, PO Box 217, 7500 AE Enschede, The Netherlands
[2] Kamerlingh Onnes Laboratory of the Leiden University, PO Box 9504, 2300 RA Leiden, The Netherlands
[3] Institute of Photonic Technology, PO Box 100239, D-07702 Jena, Germany

E-mail: j.pleikies@tnw.utwente.nl

Received 14 June 2009, in final form 14 August 2009
Published 20 October 2009
Online at stacks.iop.org/SUST/22/114007

Abstract
The sensitivity of superconducting electronics operated in the sub-Kelvin temperature range is usually limited by the hot-electron effect. Here, an increased thermal resistance due to a weakened electron–phonon coupling leads to a higher temperature of the electrons in the thin-film shunt resistors of the Josephson junctions. Cooling fins can be attached to weaken this effect. We characterized different configurations of resistors in PdAu with or without attached cooling fins by dissipating power and determining the effective electron temperature. This was done by directly measuring the Johnson noise with a SQUID amplifier. The results are compared to theory and numerical calculations on the electronic heat transport. The latter turns out to be a useful tool for the optimization of the thermal design of superconducting electronics.

1. Introduction

The thermal behavior of superconducting electronics is of special importance when a minimum noise is required at operation temperatures in the sub-Kelvin range [1–3]. We develop dc superconducting quantum interference devices (dc-SQUIDs) for the gravitational wave antenna MiniGRAIL [4], which are intended for an operation at bath temperatures T_B as low as 20 mK. This suggests a promising reachable sensitivity of the sensor, but unfortunately there is a practical limit here—the hot-electron effect [1, 5–7]. Here, the coupling between the electron and the phonon system of a resistive material is weakened. In the presence of dissipated power, this leads to an increased temperature of the electron system and therefore to an increased thermal noise of the shunt resistors of the Josephson junctions of SQUIDs [1] for example.

The hot-electron effect can be suppressed by passive cooling. This is done by so-called cooling fins (CFs) [1, 2, 8], which represent an attached reservoir for 'cold electrons'. By electronic heat transport, these extensions of the volume contribute to the thermalization of electrons.

In this paper we present an experimental and numerical study on the thermal behavior of thin-film resistors with or without attached CFs. A brief overview of some parts presented in this paper has already been published in [9].

2. Theoretical overview

2.1. Thermal resistance between the electron system and the bath

For bulk resistors, several theoretical studies on the low temperature electron–phonon interaction have been done, see for example [1, 5, 7, 10, 11]. The heat transport between the electron and the phonon system is described by

$$P = \Omega\Sigma(T_E^p - T_{Ph}{}^p). \quad (1)$$

Here, P is the dissipated power in the bulk resistor of volume Ω. Σ is a constant. T_E and T_{Ph} are the temperature of the electron and phonon system, respectively. The exponent p is dependent on the type and structure of the metal, but in general it is determined by the energy relaxation rate between the electron and the phonon system. Because the specific heat capacity of the electron system is proportional to T_E, its heat energy is proportional to T_E^2. Therefore, the energy relaxation

 © 2009 IOP Publishing Ltd Printed in the UK

rate between the electron and the phonon system is given by [7]

$$\tau_{\mathrm{EPh}}^{-1} = \alpha T_{\mathrm{E}}^{p-2}. \tag{2}$$

The constant α is determined by $\alpha = p\Sigma/\gamma$ [7]. γ is the material dependent Sommerfeld parameter which determines the heat capacity of the electron gas [12].

In many experimental cases, an exponent $p = 5$ is observed in (1) although theories partly predict differing values, see the discussion in [3, 10, 11, 13]. Depending on the disorder of the metal [11, 14] or the phonon dimensionality [10], p takes theoretical values from 4 to 6.

There exists another thermal resistance that is important in this low temperature range—the Kapitza resistance. It is caused by an acoustic mismatch of the phonon systems on interfaces between different materials that the heat flow has to pass on its way to the ambient bath [2, 3, 15]. The increased phonon temperature T_{Ph} due to the Kapitza resistance is described by

$$P = K A_{\mathrm{K}}(T_{\mathrm{Ph}}^4 - T_{\mathrm{B}}^4). \tag{3}$$

Here, the area of the interface A_{K} is used. The constant K is dependent on the involved materials. The effect of the Kapitza resistance in combination with the hot-electron effect, see (1), would also lead to an overheating of the phonon system to temperatures T_{Ph} larger than the bath temperature T_{B}. At high enough dissipated power this would also increase the temperature of the electron system T_{E} and at even higher dissipated power dominate the electron temperature. For thin-film resistors, the Kapitza resistance is usually neglected. One reason is connected to the wavelength of the thermal phonons [12]

$$\lambda_{\mathrm{Ph}} = \frac{h v_{\mathrm{S}}}{k_{\mathrm{B}} T_{\mathrm{Ph}}}. \tag{4}$$

Here, v_{S} is the speed of sound of the phonon mode, k_{B} is the Boltzmann constant and h is the Planck constant. For typical metals, v_{S} takes values of the order of 10^3 m s^{-1}. At a phonon temperature $T_{\mathrm{Ph}} = 100$ mK, this leads to $\lambda_{\mathrm{Ph}} \approx 0.5$ μm, which is larger than the thickness of typical thin films. Accordingly, a three-dimensional phonon population cannot exist. Because this is needed for the acoustic mismatch theory of the Kapitza resistance, the temperature of the phonons in the thin-film resistor is usually considered at the same temperature as the phonons of the adjacent substrate [1, 3].

2.2. Electronic thermal transport within cooling fins

From (1) it follows that a big volume Ω of the resistor suppresses the hot-electron effect. The effective volume can be increased by attaching an electrically negligible extension with volume Ω_{CF} to the resistor [1, 2, 8]. These so-called cooling fins (CFs) provide a reservoir for 'cold electrons' that exchange with the electrons in the volume of dissipation.

The total power conducted to the phonon system in these two parts of the volume is

$$P = P_{\mathrm{R}} + P_{\mathrm{CF}} = (\Omega_{\mathrm{R}} + \Omega_{\mathrm{CF}})\Sigma(T_{\mathrm{R}}^5 - T_{\mathrm{Ph}}^5). \tag{5}$$

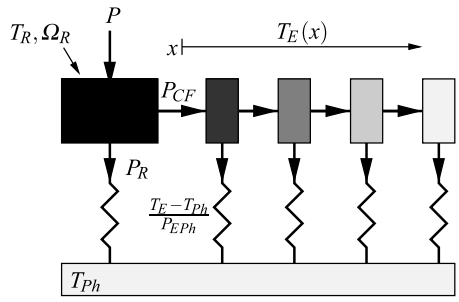

Figure 1. Simplified schematic for a resistor (on the left) with a connected one-dimensional (coordinate x) CF. The indicated thermal resistances between the electron and the phonon system (see the indicated temperatures $T_{\mathrm{E}}(x)$ and T_{Ph} respectively) are determined by (1). The power conducted to the phonon system within the resistor is indicated by P_{R} and the electronic thermal power conducted to the cooling fin is indicated by P_{CF}, see (5).

Here, we used the volume Ω_{R} of the resistor and the temperature of the electrons T_{R} in the resistor. The effective volume of the CF Ω_{CF} is a function of T_{R}, as will be shown below. Based on the preceding section, we assume a dominant hot-electron effect with the typically observed exponent $p = 5$ in (1).

The thermal transport within the geometry of such a system can be described using the Wiedemann–Franz law. It states that the thermal conductivity via the electron system of a metal is proportional to the electrical conductivity [12]. Although this is typically considered to be valid in our temperature range [12], there is another important condition. To speak of a well-defined electron temperature at one point within the volume under consideration, the length scale of the electron–electron interaction has to be small compared to typical geometries and spatial changes of the electron temperature [3]. An estimate for this length scale for a PdAu alloy, which is also employed here, is given in [16]. At a temperature of 0.1 K, with our resistivity and with data from [17], the electron–electron scattering length is below 1 μm. Accordingly, we assume that the electron temperature is spatially well defined. The total heat balance is then described by (see, for example, section II.D in [3]),

$$\frac{P}{\Omega} - \Sigma(T_{\mathrm{E}}^5 - T_{\mathrm{Ph}}^5) = -\nabla\left(\frac{\mathcal{L}}{\varrho} T_{\mathrm{E}} \nabla T_{\mathrm{E}}\right). \tag{6}$$

Here, ∇ is the nabla operator, P/Ω represents possibly dissipated power in a volume element, $\mathcal{L}$ is the Lorenz number 2.45×10^{-8} W Ω K^{-2} and ϱ the specific resistivity of the material. The Lorenz number can in practice be dependent on the material and the temperature [12]. We will ignore this fact for simplicity.

For an idealized CF, there exists an analytic solution for (6). For a negligible phonon temperature $T_{\mathrm{Ph}} = 0$ and an infinitely long CF with a constant cross-section, the spatially dependent electron temperature $T_{\mathrm{E}}(x)$ can be expressed as [2]

$$T_{\mathrm{E}}(x) = T_{\mathrm{R}}\left(1 + \frac{x}{l_{\mathrm{T}}}\right)^{-2/3} \qquad l_{\mathrm{T}} = \sqrt{\frac{14\mathcal{L}}{9\varrho\Sigma}\frac{1}{T_{\mathrm{R}}^3}}. \tag{7}$$

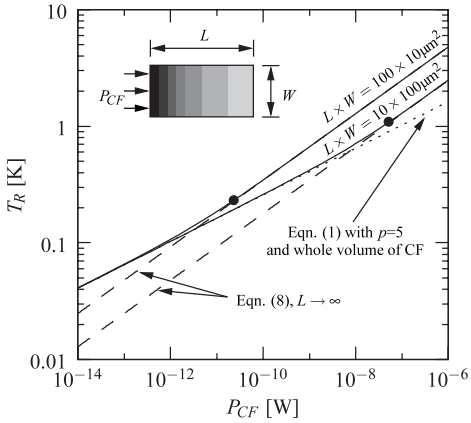

Figure 2. The solid lines show numerical calculations of the electron temperature T_R at the beginning of two linear CFs in PdAu with varying length L and width W versus the cooling power P_{CF} at $T_{Ph} = 0$. The height H, resistivity ϱ and hot-electron material constant Σ were taken from table 1. The dotted line represents (1) with $p = 5$ and the total volume of the CFs, which is identical for both CFs. The dashed lines indicate (8) for an infinitely long CF. The electron temperature T_E, where the thermal relaxation length l_T is equal to the length L of each CF (see (7)) is indicated by a solid point.

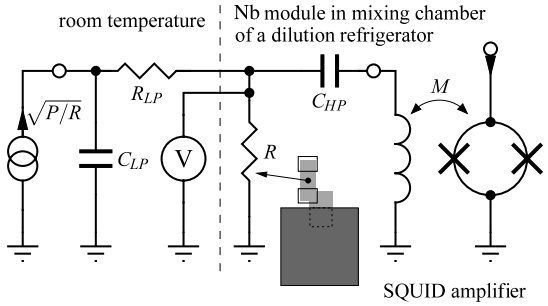

Figure 3. Measurement setup. A current source at room temperature is used to control the dissipation. The current is low-pass filtered at room temperature ($C_{LP} = 1\ \mu$F, $R_{LP} = 760\ k\Omega$) with a sub-Hz corner frequency. In the low temperature part, a capacitance $C_{HP} = 4.7\ \mu$F is connected to form a high-pass filter for the noise of the resistor R under study. This noise is measured using one of our SQUID amplifiers with a mutual inductance $M = 8.7$ nH [4].

As indicated in figure 1, T_R denotes the electron temperature in the beginning of the CF $x = 0$, which corresponds to the temperature of the electrons in the dissipating resistor. The position is defined as $x \geqslant 0$. The length scale of changes is given by l_T, which represents a *thermal relaxation length*. The total power conducted to the phonon system can be obtained from (7) by estimating the heat flux of the electron system at the beginning of the CF (see (6)),

$$P_{CF} = -A_{CF}\frac{\mathcal{L}}{\varrho}T_E(x)\frac{dT_E(x)}{dx}\bigg|_{x=0} = A_{CF}\sqrt{\frac{2\mathcal{L}\Sigma}{7\varrho}}T_R^{7/2}. \quad (8)$$

Here, the area of the cross-section A_{CF} of the CF was used. Note that the exponent of $\frac{7}{2}$ in (8) also follows from the microscopic model introduced in [1].

Equation (8) can also be expressed in terms of the electron–phonon interaction in a uniformly heated resistor of effective volume Ω_{CF} as introduced in (5). The effective volume of the cooling fin Ω_{CF} reads $\frac{3}{7}l_T A_{CF}$. Here, the temperature dependent thermal relaxation length l_T, see (7), was used. The effective volume of the cooling fin intuitively illustrates the relevance of the thermal relaxation length for the effective *cooling radius*.

In figure 2, we show a finite element method (FEM) calculation [18] of (6) on a one-dimensional CF with a finite length L. At low temperatures, the total volume of the CF is taking part in the cooling behavior. Therefore, (5) can directly be used with the total volume $\Omega_R + \Omega_{CF}$. At higher temperatures, where l_T becomes smaller than the length of the CF, the behavior is well described by the infinitely long CF. Any volume beyond a distance l_T from the dissipation area does not take part in the cooling behavior. As pointed out above, in this regime Ω_{CF} takes effective values smaller than the total volume. At even higher temperatures, the power conducted to the CF P_{CF} can become small compared to the thermal power in the resistor and the behavior is again described by (5) with only the volume of the dissipating resistor Ω_R. This can be explained by either the temperature dependency of the thermal relaxation length l_T or the lower exponent in (8) compared to the exponent $p = 5$. Note that the simple calculation in (5) only holds as long as the dimensions of the resistor are small compared to l_T. In the other case, significant temperature gradients can also occur within the volume of dissipation.

The idealized CF is useful to gain a qualitative insight into the behavior of attached cooling volumes, but in practice there are two effects that are not included. Naturally, the temperature of the phonon system should be taken into account for the case that the electron system is not completely out of thermal equilibrium. Furthermore, the actual number of dimensions the electrons can travel is of importance. Nevertheless, the thermal relaxation length l_T (see (7)) can be used to define a *cooling radius* which is, in agreement with a microscopic model [1], proportional to $T^{-3/2}$. A fraction of the resistive volume within this cooling radius takes part in the thermalization of hot electrons, it forms the volume Ω_{CF} as used in (5).

3. Heating experiments

We performed heating experiments on test structures with resistors of the typical geometrical size and resistance value of the shunt resistors attached to our SQUIDs [4, 9]. The measurements were performed in a dilution refrigerator[4], the setup is schematically shown in figure 3. The PdAu resistors are contacted by superconducting pads. By dissipating power and measuring the Johnson noise of the resistor via a SQUID, we could determine the effective electron temperature. In contrast to the measurement technique from [1, 6, 8], we employed a high-pass network between the sample and the SQUID that allows the determination and compensation of the noise of the amplifier.

[4] Leiden Cryogenics B.V., Galgewater 21, 2311 VZ Leiden, The Netherlands.

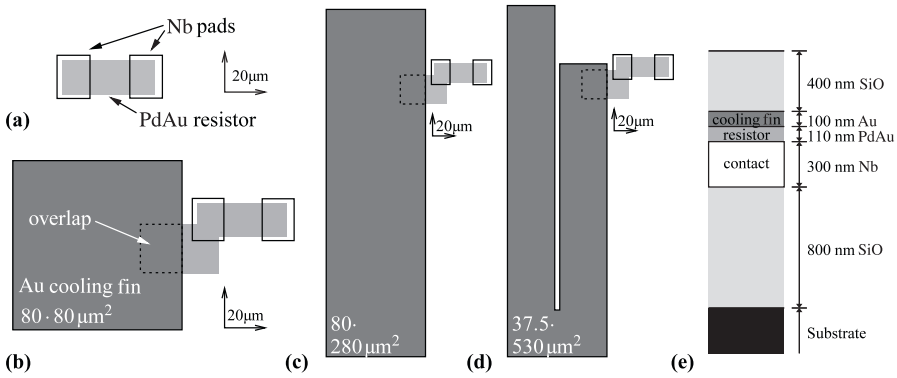

Figure 4. Layout of the different resistors with or without attached CFs. (a) Autonomous resistor in PdAu with 15 μm width. The total length is 42.5 μm and the effective length of the resistor, i.e. the spacing between the Nb contact pads, is 18.5 μm. In (b)–(d) the same resistor is extended in an electrically unimportant area and overlaps with the CF over an area of 20 × 22.5 μm^2 in all three cases. Here, electrical contact is made between the PdAu and the Au layer of the CF. CFs with varying size (b) 80 × 80, (c) 80 × 280, and (d) 37.5 × 530 μm^2 are connected. In (e), the vertical dimensions of the involved layers are shown [19], simplified as if all were stacked. The lower SiO layer is present all over the sample, whereas the upper one, a cover layer, was not present in parts of the Au CF including the overlap with the PdAu layer.

Table 1. Data of the two involved metal layers.

	PdAu	Au
Thickness H (nm)	110[a]	100[a]
Sheet resistance $R_\square$ (Ω)	3.5[b]	
Specific resistivity $\varrho = R_\square H$ (μΩ cm)	39	1.8[c]
Constant Σ with $p = 5$ (W K^{-5} m^{-3})	0.79 × 10^9 [d]	2.4 × 10^9 [7]

[a] Fabrication goal.
[b] From resistance measurements below 1 K.
[c] Parameters of the technology $\varrho_{Au} = R_\square H = 0.4\ \Omega \cdot 45$ nm [19].
[d] From fit to dissipation measurement, see section 4.

To directly study the influence of the hot-electron effect and its suppression in more detail, we added some test structures on the mask of a SQUID run in a low-T_c SQUID process [19]. Their layout is shown in figure 4. Here, resistors in the standard layer of PdAu are contacted by superconducting Nb pads. The PdAu film was deposited by RF-diode sputtering with a deposition rate of 10 nm min^{-1}. The target composition Au/Pd is 53/47 wt%. In some cases, CFs were connected to resistors of identical layout. The CFs of 80 × 80, 80 × 280 or 37.5 × 530 μm^2 area were put in a layer of Au. The reason for choosing Au was the expected better cooling behavior. The properties of the two layers are listed in table 1.

The sample with the resistor under investigation was mounted on a printed circuit board within a module made of Nb. This module was placed in the mixing chamber of a dilution refrigerator. The same module also contained the SQUID amplifier with an integrated flux transformer [4] and a high-pass capacitor, a standard part based on polyester with a room temperature capacitance of 4.7 μF. The capacitance did not drastically change when cooled down to our measurement temperatures. The measured corner frequency of the high-pass filter below 4 K was about 8 kHz.

Furthermore, it was possible to measure the voltage across the resistor by means of a pair of cables connected in a four-point configuration. Below bath temperatures of 1 K, we measured resistances close to 4.4 Ω for all the different characterized resistors. These values were only a few per cent lower than the ones measured at 4.2 K. This corresponds to a sheet resistance of 3.5 Ω, whereas the goal of fabrication was 4 Ω. It is not clear if this variation originated from either a changed thickness H of the PdAu layer, a difference in the resistivity, or a mixed situation. For simplicity, we addressed the comparably small deviation in sheet resistance to a change in resistivity and assumed the goal thickness of the layer of 110 nm as the fabricated thickness, see table 1.

The SQUID was directly coupled to a SQUID-electronics[5] and the noise spectrum was determined in a flux-locked loop. The employed high-pass scheme allows us to easily bias the resistor with a constant current. Furthermore, we could also measure the noise of the SQUID readout in the low frequency region and subtract its noise power spectral density (PSD). A typical noise measurement is depicted in figure 5(a). The effective temperature of the electron system in the shunt resistor was determined by

$$T_E = \frac{R}{4k_B M^2}\left(S_{\Phi,HF} - S_{\Phi,VV} - \frac{4k_B \cdot 300\ \mathrm{K} \cdot M^2}{R_{LP}}\right). \quad (9)$$

Here, $S_{\Phi,HF}$ is the flux noise PSD between 90 and 100 kHz and $S_{\Phi,VV}$ is the effective additional flux noise PSD of the SQUID. R is the measured value of the resistor and M is the mutual inductance between the SQUID inductance and its input coil. The last term represents the subtracted noise PSD of the room temperature low-pass resistance $R_{LP} = 760$ kΩ, which is not present in the low frequency range, see figure 3. Because we simply used the SQUID in a single-stage setup, the flux noise of the SQUID of typically 1.5 $\mu\Phi_0/\sqrt{\mathrm{Hz}}$ was dominated by the input voltage noise of the readout electronics. Φ_0 is the magnetic flux quantum 2.07 × 10^{-15} Wb.

During all the measurement series shown below, we first stabilized the temperature of the dilution refrigerator and recorded the value from an integrated thermometer. Then we measured the resistance R, using comparably small currents,

[5] Supracon AG, Wildenbruchstr. 15, 07745 Jena, Germany.

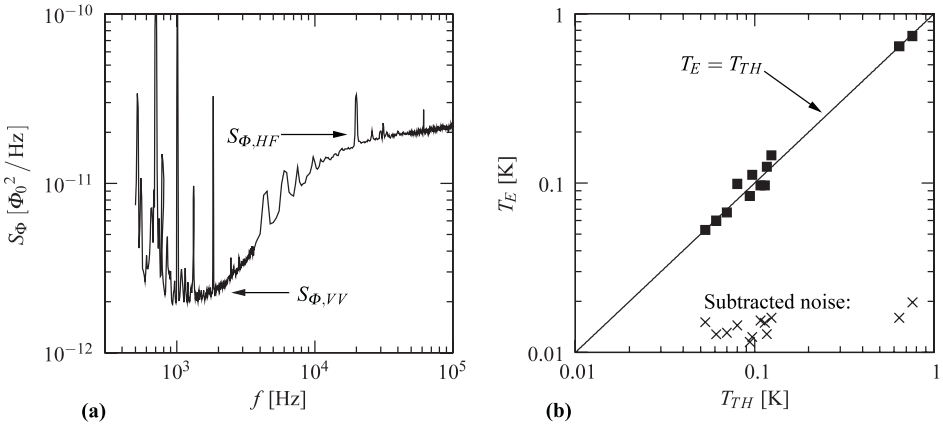

Figure 5. (a) Typically measured SQUID flux noise spectrum, here at a temperature of 84 mK. The noise peaks at the lower frequencies were mainly caused by mechanical vibrations that could not be damped and the high frequency peaks were most probably of both mechanical and electromagnetic origin. The two important noise levels are indicated, see (9). (b) Comparison of the measured bath temperatures for the later shown measurement series, determined by either the integrated thermometer or the SQUID. T_{TH} is the temperature determined from a thermometer integrated in the dilution refrigerator. T_{E} is determined from the measured SQUID spectra without a dissipation with (9), where the 'x' markers show the equivalent temperature of the subtracted noise of the readout system. See the second and third term of (9), the marker '$S_{\Phi,\mathrm{VV}}$' in (a) and the text for more details.

and measured the noise spectrum of the SQUID to determine the temperature without power dissipation. Then we gradually changed the current through the resistor and recorded the dissipated power–electron temperature characteristics ($P = RI^2$). In the end of each series we verified that the bath temperature did not change during the measurement.

Figure 5(b) depicts a comparison of the bath temperatures determined by the two different methods. The result suggests that there is no systematic error between the values measured via the SQUID or via the thermometer. The differences can be explained by a thermal gradient within the mixing chamber: the integrated thermometer was situated at a distance of about 10 cm from the Nb module that contained the sample. Furthermore, the graph shows that the noise of the readout system (see the subtracted terms in (9)) is not dominant but of importance for an accurate determination of the electron temperature.

4. Experimental results on an autonomous resistor

The results for the resistor without CF are shown in figure 6. The bath temperatures T_{B} are the values determined from the SQUID measurement without dissipation. We fitted the measurement data to (1). Here, we only used the data from the lower range of power dissipation P, up to about 1 nW. The resulting exponent of $p = 5.05$ is in accordance with most experiments on metals in the clean and dirty limit, see section 2.1. Our sample was certainly in the *dirty limit*. In [20], an estimate for the mean free path of the electrons $l_{\mathrm{E}} \approx 2$ nm of an PdAu layer with a similar resistivity is given. In [21], the speed of sound v_{S} is estimated to 3.5×10^3 m s^{-1} for the longitudinal and 1.3×10^3 m s^{-1} for the transverse phonons in PdAu, respectively. The expression $2\pi l_{\mathrm{E}}/\lambda_{\mathrm{Ph}}$ yields, with (4) and the minimum bath temperature of 100 mK, a value of about 10^{-3}: the dirty limit. Accordingly, our observed exponent $p \approx 5$ is another example for experimental results that are in discrepancy with existing theories. We will come back to this below.

Because the resistor is contacted by a superconductor, hot electrons stay within the resistive volume due to Andreev reflection. The superconducting electrodes limit the dissipative area of the resistor by the distance between them. Nevertheless, the electron–phonon relaxation takes place in the whole resistor volume including the parts covered with Nb. The influence of the possible proximity effect on the resistor film [3] can be neglected in our case due to the relatively large film thickness and the short mean free path of electrons in PdAu. This assumption is confirmed by the fact that thermal power is transferred through the covered part of the resistor to the CFs, as will be shown below.

The fit of (1) with a constant exponent $p = 5$ is shown in figure 6. Using the total volume of the resistor we were able to estimate the hot-electron material constant Σ_{PdAu} for the PdAu layer with a resistivity of 39 $\mu\Omega$ cm to 0.79×10^9 W K^{-5} m^{-3}.

In [21], the Sommerfeld parameter γ for a PdAu alloy is experimentally determined to 3.88 mJ mol^{-1} K^{-2}. Using standard values for the density and atom mass, this leads to an electronic heat capacity in PdAu of about 400 J m^{-3} K^{-2} $\cdot\, T_{\mathrm{E}}$. With (2), this allows us to estimate the characteristic electron–phonon scattering time τ_{EPh} in our experiment to $\approx 10^{-7}$ s K^3 $\cdot$ T_{E}^{-3}. At the minimum observed electron temperatures of about 100 mK (see figure 6) the electrons emitted energy to the phonon system in scattering processes that took place every 0.1 ms on average.

We also performed measurements at higher bath temperatures. The measurement data of all series in a higher temperature regime are depicted in figure 7. At higher dissipated power $P \gg 1$ nW, the exponent p deviates from the low power regime, see figure 7. The measurement at $T_{\mathrm{B}} = 740$ mK follows $p \approx 4.4$. We have two possible explanations for this deviation.

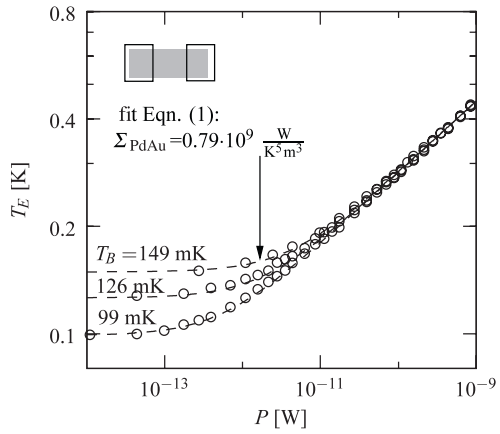

Figure 6. Measurement on the autonomous resistor for different bath temperatures T_B. The dissipated power P is plotted versus the electron temperature T_E. The dashed lines are the fit to (1) with $p = 5$. Σ was determined with the complete volume of the resistor including the parts covered with Nb.

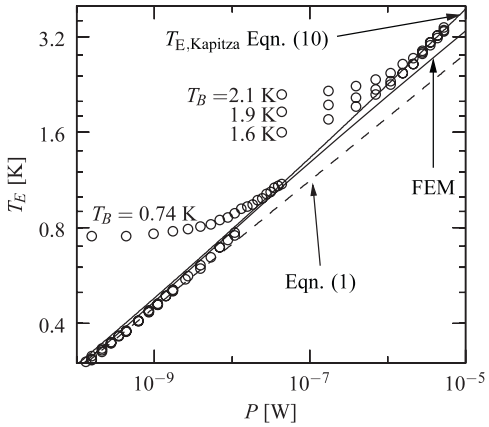

Figure 7. The measured data on the autonomous resistor at the higher temperature regime; compare this with figure 6. The three measurements at the highest bath temperatures T_B were performed in a vacuum-pumped ^{4}He bath-cryostat. The fit for the low power regime is also here shown as a dashed line. The solid line marked with 'FEM' is the numerical calculation of (6) with $T_{Ph} = 100$ mK and the data from table 1. The electron temperature with influence of the Kapitza resistance $T_{E,Kapitza}$ is calculated with (10) with the total area of the resistor, $T_B = 0$ and $K = 80$ W m^{-2} K^{-4}, which was chosen to fit the data at the highest temperatures.

First of all, the length of the Nb covered parts of the resistor is equal to the thermal relaxation length l_T at $T_E = 1$ K, see (7). Accordingly, these parts of the volume do not fully participate in the cooling above this temperature. An FEM calculation [18] of (6) on the real geometry of the resistor is shown in figure 7. We defined the geometry in two dimensions with the data for PdAu from table 1. Simulating the real measurement, we only dissipated power in the area A_R between the Nb connectors. Then we calculated the spatial average of the electron temperature $T_E(x, y)$ over the area between the connectors $T_R = A_R{}^{-1} \int\int T_E(x, y)\mathrm{d}x\,\mathrm{d}y$. T_R corresponds to the effective temperature one would observe in a noise measurement. The result for varying power is shown in figure 7 as the solid line marked with 'FEM'. As one can see, the calculation deviates as expected from the fit for the resistor, which is shown as a dashed line. At much higher temperature, the behavior is described by a solution of (1) with an exponent $p = 5$ and the volume between the contact pads only. Nevertheless, the measured deviation at even higher temperatures is not well explained.

Another influence at high power could be given by the Kapitza resistance. Combining (1) and (3) leads to

$$T_{E,Kapitza} = \sqrt[5]{\frac{P}{\Sigma H A_R} + \left(\frac{P}{K A_R} + T_B^4\right)^{5/4}}. \qquad (10)$$

We also plotted this noise contribution in figure 7. This could be an explanation for the high temperature deviation. At low temperatures, the Kapitza resistance is of vanishing influence and its existence at the boundary between the resistor and the surrounding SiO substrate is doubtful. As already pointed out in section 2.1, a requirement for the Kapitza resistance is that two distinct phonon populations must exist in the adjacent materials. With (4) and the above given data for the speed of sound in PdAu, one can estimate that the wavelength of the phonons λ_{Ph} becomes larger than the thickness of the resistive layer at temperatures below 1.5 K for the longitudinal and below 0.6 K for the transversal phonon system, respectively. Therefore, the phonon population in the resistor should be two-dimensional in our measurement regime. The theory concerning the Kapitza resistance is based on three-dimensional phonon populations [15].

The phonon dimensionality could have another effect. According to [10], the exponent p in (1) changes when the phonon wavelength becomes comparable to the film thickness. Thick-film resistors of the same alloy but with clearly three-dimensional phonons were characterized in [17]. Here, an exponent $p = 4$ was observed with a $\Sigma \propto \varrho^{-1}$ dependency [17]. This case is not explained by any of the existing theories [13]. Another reported measurement on PdAu thin-film resistors shows an exponent $p = 5$ in a range of resistivity and temperature similar to our experiment [20]. We conclude that the electron–phonon coupling in our two-dimensional phonon case could be of a bulk $p = 4$ dependence [17] affected by the phonon dimensionality in the sense of the work presented in [10].

5. Resistors with cooling fins

We repeated the same experiment on three different configurations of resistors with attached CFs, see figures 4(b)–(d). To compare our measurement data with the theory of the electronic thermal transport, we again performed FEM calculations on (6) in two dimensions.

In the calculation, the phonon temperature T_{Ph} was assumed to be equal to the bath temperature T_B over the whole geometry and to be independent of the power. Naturally, the dissipation term in (6) was only applied in the area between the contact pads. The respective parts of the geometry were modeled with the values from table 1. In the overlapping area of PdAu and Au, $d_{Au}\Sigma_{Au} + d_{PdAu}\Sigma_{PdAu}$ and $d_{Au}/\varrho_{Au} +$

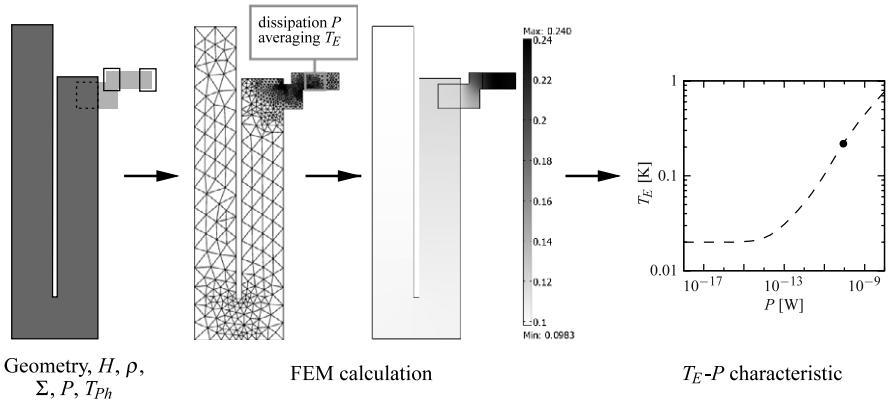

Figure 8. Illustration of the FEM calculation on (6). The geometry and important parameters (see table 1) are used to define the model. The dissipation P is only active in the indicated area of the resistor. The third picture from the left shows an exemplary FEM calculation with $P = 0.1$ nW and a phonon temperature T_{Ph} of 20 mK. The gray scale represents the electron temperature T_{E} from 0.1 K (white) to 0.24 K (black). For the dissipated power–electron temperature characteristic, the electron temperature is spatially averaged over the area of the resistor.

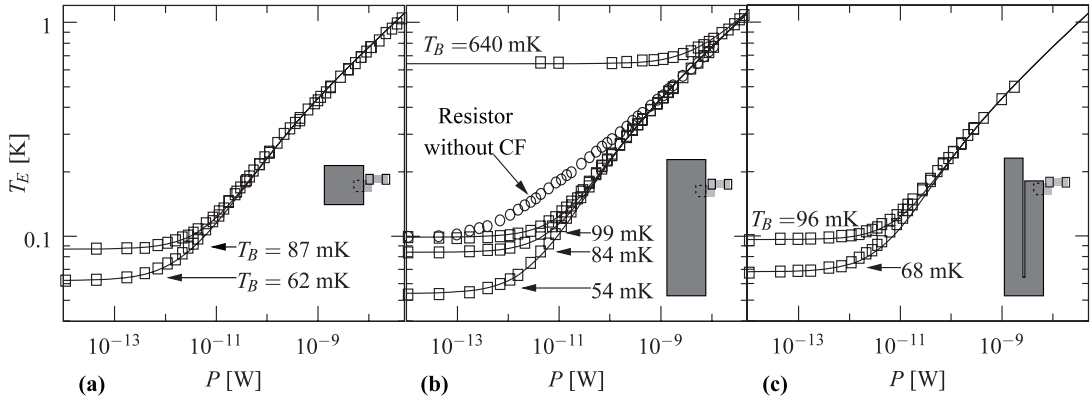

Figure 9. (a)–(c) Measurement data for different bath temperatures T_{B} (squares) on resistors with varying CFs, see figure 4. The dissipated power P is plotted versus the electron temperature T_{E}. The solid lines are FEM calculations on the accurate geometry of each configuration and the bath temperature derived from the measurement. In (b), we also plotted one measurement series of the autonomous resistor from figure 6 (circles).

$d_{\mathrm{PdAu}}/\varrho_{\mathrm{PdAu}}$ were used in the respective terms. To estimate the effective electron temperature of the resistor for each dissipated power, the temperature was averaged in the area between the Nb connectors. The calculations are illustrated in figure 8.

Both the FEM calculations and the measurement data for all three configurations are shown in figure 9. Note that the only fit used is the one from the last section, the determination of Σ_{PdAu}. The agreement is very good, which suggests that our experiment is well described by the electronic thermal transport model. In particular, the data for the PdAu layer and the theoretical Lorenz number $\mathcal{L}$ seem to be close to the real values.

From figure 9(b) one can see that the connected CF lowers the temperature as expected. This supports the conclusion that the superconducting proximity effect in the area covered by Nb can be neglected, see the experimental results on the autonomous resistor from section 4. Above a dissipated power of about 100 pW, which is also about the power dissipation of the SQUIDs that were fabricated on the same wafer [4], the additional cooling effect vanishes.

We performed FEM calculations on the different configurations to make the comparison of the different CFs easier. The result is shown in figure 10. The two CFs of area $80 \times 280\ \mu\mathrm{m}^2$ and $37.5 \times 530\ \mu\mathrm{m}^2$, thus with a comparable volume, show about the same behavior. The smaller CF $80 \times 80\ \mu\mathrm{m}^2$ shows a slightly smaller cooling power. We have to conclude that we could not clearly see a difference between the different attached CFs in Au. First we intended to measure differences according to the dimensionality of the Au fin. Unfortunately, we underestimated the screening of the weak thermal PdAu connection to the CF. The thermal relaxation length l_{T}, see (7), for our employed PdAu layer (see table 1) yields $11\ \mu\mathrm{m\ K}^{3/2} \cdot T_{\mathrm{R}}^{-3/2}$. If one approximates the connecting parts to the Au CF to be a one-dimensional CF as treated in section 2.2, the distance to the beginning of the Au CF is roughly 30 μm. l_{T} becomes smaller than this value at temperatures $T_{\mathrm{E}} \gtrsim 0.5$ K. Above this temperature there is no influence of material connected beyond that distance, see section 2.2. A comparison of the calculation of the resistor with and without CFs in figure 10 supports this insight.

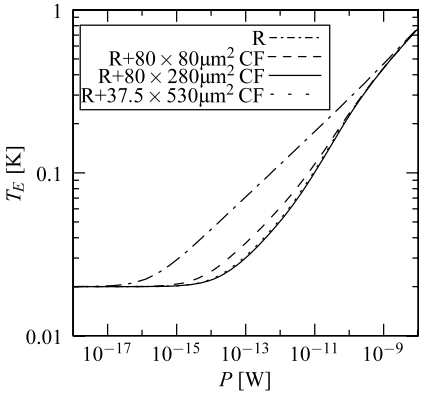

Figure 10. FEM calculations on all the characterized configurations at a phonon temperature T_{Ph} =20 mK. Note that the solid and the dotted line are almost identical.

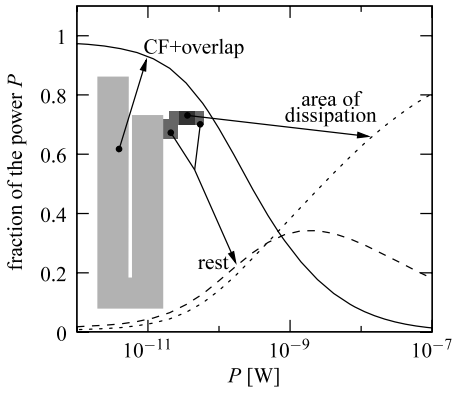

Figure 11. Illustration to show where within the geometry the largest fraction of the power is drained to the phonon system. This is calculated by $\frac{1}{P}\int\int H\Sigma(T_{\mathrm{E}}(x,y)^5 - T_{\mathrm{Ph}}{}^5)\mathrm{d}x\,\mathrm{d}y$ within each of the indicated parts. The phonon temperature T_{Ph} is 20 mK.

In figure 11, we show a calculation that indicates in which parts of the geometry the dissipated power is drained to the phonon system. At low dissipated power P, the whole volume participates in the cooling. This corresponds to the data for $P \lesssim 10^{-11}$ W in figure 11. Here, the larger fraction of the dissipated power is drained within the CF. This is due to the fact that the CF also covers the largest fraction of the total volume. At intermediate dissipated power, the cooling volume is restricted in the sense of the temperature dependent thermal relaxation length, see (7). At high dissipation $P \gtrsim 10^{-8}$ W, the largest fraction of the power is drained within the volume of dissipation. The three regimes as mentioned in section 2.2 are present in the calculation. The intermediate and high power regimes can also be clearly identified in the measurement data, see the comparison of the experimental data on resistors with and without the CF in figure 9(b). The low power regime is not accessible in the bath temperature range of our and other [1, 8] measurements on resistors with attached CFs.

A fit of the measurement data on the resistors with CFs to (1) leads to an apparent lower exponent $p \approx 2.5$ in the lower range of power dissipation. This is in agreement with other measurements on resistors with CFs [1, 8]. According to the simple non-uniform heating model described in [1], this is caused by a diffusion of hot electrons into a cooling volume of one to two dimensions. This is a good approximation of our geometry.

6. Conclusions

The heating experiments on PdAu thin-film resistors with possibly attached cooling fins give insights into the thermal behavior and therefore into the optimization of such structures. The measurements on resistors with attached CFs could be well reproduced by FEM calculations based on the theory of the hot-electron effect and the thermal transport via the electrons within the geometry of the system. This turns out to be a powerful tool to predict the minimum reachable electron temperature and therefore the optimum reachable sensitivity of superconducting electronics cooled to the sub-Kelvin temperature range.

We want to give a qualitative guideline for a minimization of the effective electron temperature in resistors with attached CFs. First of all, the volume of the resistor itself has to be maximized. Here, one has to be careful that the damping effect of the shunt resistor of the Josephson junction is maintained. If there is a choice of material, Σ should also be maximized. Naturally, this directly lowers the electron temperature of the resistor and the temperature on the boundary to an adjacent cooling volume. This has the additional effect of an increased thermal relaxation length (see (7)) which in turn makes larger parts of an attached cooling fin accessible. Furthermore, the largest possible amount of metal should be situated as close as possible to the volume of dissipation. The effective cooling radius is given by the thermal relaxation length. A material with a lower resistivity further increases this length scale.

References

[1] Wellstood F C, Urbina C and Clarke J 1994 Hot-electron effects in metals *Phys. Rev.* B **49** 5942–55
[2] Savin A M, Pekola J P, Averin D V and Semenov V K 2006 Thermal budget of superconducting digital circuits at subkelvin temperatures *J. Appl. Phys.* **99** 084501
[3] Giazotto F, Heikkilä T T, Luukanen A, Savin A M and Pekola J P 2006 Opportunities for mesoscopics in thermometry and refrigeration: physics and applications *Rev. Mod. Phys.* **78** 217
[4] Pleikies J, Usenko O, Kuit K H, Flokstra J, de Waard A and Frossati G 2007 SQUID developments for the gravitational wave antenna MiniGRAIL *IEEE Trans. Appl. Supercond.* **17** 764–7
[5] Gantmakher V F 1974 Experimental study of electron–phonon scattering in metals *Rep. Prog. Phys.* **37** 317–62
[6] Roukes M L, Freeman M R, Germain R S, Richardson R C and Ketchen M B 1985 Hot electrons and energy transport in metals at millikelvin temperatures *Phys. Rev. Lett.* **55** 422–5
[7] Echternach P M, Thoman M R, Gould C M and Bozler H M 1992 Electron–phonon scattering rates in disordered metallic films below 1 K *Phys. Rev.* B **46** 10339–44

[8] Vinante A, Falferi P, Mezzena R and Mück M 2007 Hot-electron effect in palladium thin films *Phys. Rev.* B **75** 104303
[9] Pleikies J, Usenko O, Frossati G and Flokstra J 2009 SQUID current amplifiers for sub-kelvin operation temperatures *Cryogenics* at press (doi:10.1016/j.cryogenics.2008.12.020)
[10] Qu S X, Cleland A N and Geller M R 2005 Hot electrons in low-dimensional phonon systems *Phys. Rev.* B **72** 224301
[11] Sergeev A and Mitin V 2000 Electron–phonon interaction in disordered conductors: static and vibrating scattering potentials *Phys. Rev.* B **61** 6041–7
[12] Kittel C 1996 *Introduction to Solid State Physics* 7th edn (New York: Wiley)
[13] Lin J J and Bird J P 2002 Recent experimental studies of electron dephasing in metal and semiconductor mesoscopic structures *J. Phys.: Condens. Matter* **14** 501–624
[14] Jan W, Wu G Y and Wei H S 2005 Electron–lattice interaction in impure metals *Phys. Scr.* **71** 552–5
[15] Lounasmaa O V 1974 *Experimental Principles and Methods Below 1 K* (New York: Academic)
[16] Lin J J and Giordano N 1987 Localization and electron–electron interaction effects in thin Au–Pd films and wires *Phys. Rev.* B **35** 545–56
[17] Zhong Y L and Lin J J 1998 Observation of a linear mean-free-path dependence of the electron–phonon scattering rate in thick AuPd films *Phys. Rev. Lett.* **80** 588–91
[18] *Comsol Multiphysics Version 3.3* 2007 FEM software, Comsol Inc., Stockholm, Sweden
[19] IPHT Jena e.V. 2008 *Correspondence and Design Rules LTS SQUID process* (Department of Quantum Electronics, Postfach 100239, 07702 Jena, Germany) online available at http://www.ipht-jena.de/uploads/media/a13_ipht_squid_1_4_04.pdf
[20] Kanskar M and Wybourne M N 1994 Crossover between dissipative and nondissipative electron transport in metal wires *Phys. Rev. Lett.* **73** 2123–6
[21] Yeh S S, Lin J J, Xiunian J and Dianlin Z 2005 Electron–phonon-impurity interference effect in disordered $Au_{56}Pd_{44}$ and IrO_2 thick films *Phys. Rev.* B **72** 24204